Spontaneous Formation of Vesicles of Diblock Copolymer EO_6BO_{11} in Water: A SANS Study†

Alexander I. Norman,*,‡,# Derek L. Ho,§ Jae-Ho Lee,⊥ and Alamgir Karim‡

Polymers Division, Stop 8542, National Institute of Standards and Technology, 100 Bureau Drive, Gaithersburg, Maryland, 20899, Center for Neutron Research, Stop 8562, National Institute of Standards and Technology, 100 Bureau Drive, Gaithersburg, Maryland, 20899, and Department of Chemical Engineering, University of Maryland, College Park, Maryland, 20742

Received: August 8, 2005; In Final Form: November 4, 2005

Small angle neutron scattering (SANS) is used to study the structures formed in water by a diblock copolymer EO_6BO_{11} (having 6 ethylene oxide, EO, and 11 butylene oxide, BO, units). The data show that polymer solutions over a broad concentration range (0.05−20 wt %) contain vesicular structures at room temperature. Interestingly, these vesicles could be formed without any external energy input, such as extrusion, which is commonly required for the formation of other block copolymer or lipid vesicles. The EO_6BO_{11} vesicles are predominantly unilamellar at low polymer concentrations, whereas at higher polymer concentrations or temperatures there is a coexisting population of unilamellar and multilamellar vesicles. At a critical concentration and temperature, the vesicular structures fuse into lyotropic arrays of planar lamellar sheets. The findings from this study are in broad agreement with the work of Harris et al. (*Langmuir*, **2002**, *18*, 5337), who used electron microscopy to identify the vesicle phase in the same system.

Introduction

Vesicles are, potentially, excellent candidates for controlled release vehicles. Applications of such materials include pharmaceuticals, agricultural applications, and personal care products.[1−3] Many groups, over the past decade, have studied the aqueous behavior of a range of ethylene oxide/butylene oxide (EO_mBO_n) diblock copolymers (where n and m are the number of repeat units).[4−9] Similar systems containing $EO_mPO_nEO_m$ (ethylene oxide/propylene oxide/ethylene oxide) triblock copolymers have been observed, by small-angle light scattering (SALS), small-angle neutron scattering (SANS), birefringence, and rheology, to form multilamellar vesicles (MLVs) in water when subjected to shear.[10,11] These multilamellar vesicles, often referred to as "onions", were formed from shearing a relatively low concentration (21% by mass fraction) of a commercial EO_n-PO_mEO_n block copolymer (Pluronic P123, where $n = 20$ and $m = 70$) in a mixture of water and 1-butanol. The increase in viscosity and the characteristic four-lobe SALS pattern were signatures of such phases. [12,13] The formation of MLVs (often referred to as liposomes) is extremely common in phospholipids; however, they are subject to limitations in their chemical and mechanical abilities, e.g., unstable in higher pH and following extrusion.[14] Diblock copolymers comprised of ethylene oxide and ethyl ethylene units form MLVs that display greater mechanical stabilities than the MLVs formed from phospholipids. [15] This evidence suggests that vesicles formed from EO_n-BO_m diblock copolymers may also display mechanical stabilities that are substantially greater than phospholipids.

Similar structures have been found for block copolymers of polystyrene (PS)-*b*-poly(ethylene oxide) (PEO) in water,[16] and polystyrene (PS)-*b*-poly(acrylic acid) (PAA) in solvent mixtures of dioxane/THF/H_2O and DMF/THF/H_2O.[17] The formation of such structures has been described in terms of the interfacial energy between the core and the solution, the stretching of the blocks within the core, and the repulsive interactions between chains in the corona.[18,19] These structures can be characterized by polarized light microscopy. The typical textures observed are Maltese cross patterns, which are typically observed for spherulites during polymer crystallization.[20,21] Polarized light microscopy measurements alone, however, cannot distinguish between ULVs and MLVs.

A model proposed by Israelachvili et al. [22] estimates the stability of the vesicle phase. The critical packing factor ϕ is estimated as:

$$\phi = \frac{V}{l_c a_0} \tag{1}$$

where V is the hydrophobe volume, a_0 is the cross sectional area of the hydrophilic headgroup at the surface, and l_c is the hydrophobe length. At values of $\phi \sim 0.5-1$, lamellae form. These lamellae can be either planar or vesicular. The morphology can be tuned by changing the length of the respective blocks. The value of ϕ can be adjusted by increasing the length of the EO group (providing that the length of the BO group remains the same), for example, spherical micelles are shown to exist as the extent of curvature increases. [23,24] Reverse structures have been observed for values of $\phi \geq 1$. [25] Systems which form bilayers show that with increasing concentration there is a structural progression from vesicles to planar bilayers.[25] Regev and Guillemet[26] observed such a phenomenon for the nonionic surfactant, cocodiethanolamide.

Harris et al.[27] demonstrated that vesicles are formed spontaneously in mixtures of EO/BO diblock copolymers (specifi-

* Address correspondence to this author.
† Contribution from the National Institute of Standards and Technology.
‡ Polymers Division, National Institute of Standards and Technology.
# Present address: Department of Chemistry and Biochemistry, University of Maryland, College Park, Maryland, 20742.
§ Center for Neutron Research, Stop 8562, National Institute of Standards and Technology.
⊥ University of Maryland.

10.1021/jp0544336 CCC: $33.50
Published on Web 12/14/2005

cally EO_6BO_{11}, EO_7BO_{12}, $EO_{11}BO_{11}$, and $EO_{14}BO_{10}$) and water. The majority of the more detailed analyses were performed on $EO_{11}BO_{11}$. Unlike most copolymers, there was no requirement for specialized procedures or external energy inputs to observe these structures. The vesicles formed were multilamellar and were stable after sonication, moderate and high shear mixing, and extrusion. The stability of these vesicles is a result of many factors: The polar ethylene oxide headgroup is solvated via hydrogen bonding to the surrounding solvent (water). This hydration shell forms a barrier to vesicle degradation. Collisions are likely to occur between the vesicles but this is not likely to penetrate the vesicle shell. The hydrophobic butylene oxide block enhances the stability due to the ethyl branching along the chain, providing greater entanglement between hydrophobes, explaining why such polymers form vesicles of greater mechanical stability than phospholipids. Since this polymer forms vesicles so easily under such favorable conditions (at room temperature, in water), it is a prime candidate for biological encapsulation applications.

Our work uses small-angle neutron scattering (SANS) in an attempt to show the vesicle structure of one of these copolymers: EO_6BO_{11} in aqueous solution. We compare our findings to those from Harris et al.[27] Our findings show broad agreement with conclusions drawn from microscopy methods by Harris et al.[27] We also discuss the effect of polymer composition and temperature on the vesicles of EO_6BO_{11} in water.

Theory

For a system of particles the scattered intensity is given as:

$$I(q) = n\Delta\rho^2V^2P(q)S(q) \tag{2}$$

where n is the number density of the particles, $\Delta\rho$ is the difference in scattering length density, V is the volume of particles, $P(q)$ is the form factor, and $S(q)$ is the structure factor, where the wavenumber $q = 4\pi \sin\theta/\lambda$ (2θ is the scattering angle and λ is the wavelength of the incident radiation).

The form factor is a function describing the intraparticle scattering from the *shape* of the scattering particles. The form factor has been calculated for spheres, rods, and lamellae and the interested reader is referred to the literature.[28−32]

The intermediate range of the profile is the region in which the form factor contains information regarding particle size and shape. In this regime the scattering results from the dimensionality of the scattered particle, for example, the scattered intensity of a rodlike micelle scales as q^{-1}, whereas a vesicle shell or a disk scales as q^{-2}.[33]

This paper focuses on the formation of vesicles and we will concentrate on the approximations to the scattering curves that are available for such systems. The scattered intensity, $I(q)$, can be modeled in terms of the form factor, $P(q)$, of noninteracting scattering particles (that is when $S(q) \rightarrow 1$ and is therefore negligible to the overall observed scattering, $I(q)$). The form factor, $P(q)$, from ULVs of radius R and bilayer thickness t, is:[34]

$$P(q) = (\Delta\rho^2)\left\{\frac{4}{3}\pi R^3\frac{3J_1(qR)}{qR} - \frac{4}{3}\pi(R+t)^3\frac{3J_1[q(R+t)]}{q(R+t)}\right\}^2 \tag{3}$$

where J_1 is a first-order Bessel function.

For thin bilayers ($t \ll R$), or for large vesicles, $P(q)$ becomes:

$$P(q) = (\Delta\rho^2)(4\pi R)^2\frac{t^2}{q^2}\sin^2(qR) \tag{4}$$

Equation 4 indicates that for large, noninteracting vesicles, $I(q)$ should show a q^{-2} decay in the low q regime. This equation shows two q dependent oscillations in the observed scattering: (1) A fast oscillation that is dependent on the radius (R) of the vesicle and (2) a slow oscillation that is dependent on the thickness of the vesicle membrane. The fast oscillations may become smeared out when there is a substantial polydispersity in the vesicle radius. The Kratky−Porod approximation[35] utilizes the Fourier transformation of the scattering length density profile through the membrane and is defined in eq 5.

$$P(q) = \rho^2\left[\frac{2}{q^2}\sin\left(\frac{1}{2}qt\right)\right]^2 \tag{5}$$

Generalized Indirect Fourier Transformation (GIFT). The observed scattered intensity is related to the pair distance distribution function (PDDF), $p(r)$, by the Fourier transformation[34]

$$I(q) = 4\pi\int_0^\infty p(r)\frac{\sin(qr)}{qr}\mathrm{d}r \tag{6}$$

where the PDDF, $p(r)$, is given by

$$p(r) = r^2\Delta\tilde{\rho}^2(r) = \frac{1}{2\pi}\int_0^\infty I(q)(qr)\sin(qr)\,\mathrm{d}q \tag{7}$$

where $\Delta\tilde{\rho}^2(r)$ is the convolution square of $\Delta\rho(r)$, the scattering density difference, averaged over all directions in real space. This function is used to determine size, shape, and flexibility of scattered particles. The $p(r)$ function is defined as the probability of finding a distance, r, between any pair of volume elements, of the scattered particle weighted with the product of the scattering length densities of the two volume elements. The calculation of $p(r)$ requires SANS data over the q range 0 to ∞. Our limited q range would lead to strong oscillations in such a direct Fourier transform. The $p(r)$ is calculated by using a technique termed "generalized indirect Fourier transformation" (GIFT).[34] GIFT solves this problem with a model-free, iterative algorithm that simultaneously performs least-squaresd fitting, smoothing, desmearing, and Fourier transformation assuming a limitation in $p(r)$, i.e., $p(r) = 0$ for $r > D_{max}$ (where D_{max} is the maximum dimension of the scattered particle). The GIFT calculation is part of the commercially available PCG software (Version 1.01.02).

Experimental Section

Synthesis and Characterization of Polymers. The diblock copolymer EO_6BO_{11} was synthesized by sequential anionic polymerization of 1,2-butylene oxide and ethylene oxide. We obtained this polymer as a gift from the Dow Chemical Company. Full details on the polymer synthesis and characterization have been described elsewhere.[27,36]

Vesicle Preparation. Neat block copolymer was added to D_2O until the desired concentration was reached. The sample vial was shaken by hand for approximately 120 s. Aqueous dispersions were prepared in 0.025% (by mass fraction), 0.05%, 0.5%, 5.0%, and 20.0% concentrations. Samples were filtered and allowed to stand for a minimum of 48 h before any analysis was performed.

Small-Angle Neutron-Scattering (SANS) Measurements. SANS experiments were carried out with use of the NG7 30 m SANS instrument at the National Institute of Standards and Technology (NIST) Center for Neutron Research (NCNR), Gaithersburg, MD.[37]

Three instrumental settings were used to cover the wavenumber range 0.0009 $Å^{-1} \leq q \leq 0.5548$ $Å^{-1}$. The three settings of wavelength and sample-to-detector distance used to achieve this were 8.09 Å and 15.3 m (with the focusing lens configuration), 6.0 Å and 6.0 m, and 6.0 Å and 1.1 m, with a wavelength resolution of $\Delta\lambda/\lambda = 0.11$. The scattered intensity was corrected for background and parasitic scattering,[38] placed on an absolute scale using a calibrated secondary standard, and a radial average was performed to yield the scattered intensity, $I(q)$, as a function of the wavenumber, q, in one dimension. Finally the low incoherent background was subtracted. This was determined from the asymptotic slopes of $I(q)\cdot q^4$ vs q^4.[39] This was done for each sample at each different temperature. All solutions were prepared in D_2O, which provides a low incoherent background and strong contrast. The resulting samples were filtered and then loaded into quartz cells of 1 mm path length. The five samples prepared were investigated at temperatures between 10 and 90 °C. Due to time restrictions, not all experiments were probed to such a low q range. The experiments in which this was the case probed a q range of 0.0053 to 0.5548 $Å^{-1}$. The sampling time depends on how many counts per second hit the detector. This time depends on the configuration of the instrument (whether it uses the focusing lens, the high q configuration, or the low q configuration), the sample concentration, and the sample temperature. Typically, the lower concentration samples required a longer acquisition time than those at a higher concentration. On increasing the temperature, it was possible to reduce the acquisition time. The maximum acquisition time for one sample was 1 h (0.025% mass fraction at 50 °C, using all three configurations), with the lowest being 10 min (20% mass fraction at 20 °C, using only high and low q configurations). The error (standard uncertainty) associated with the SANS experiments is dependent on various factors, such as the detector count rate, the estimation in conversion of pixel number to scattering vector, and the secondary standard. Such errors are calculated automatically in the software used for SANS data collection. For clarification purposes, the error bars in some of the figures have been omitted.

The SANS data were modeled to a polydisperse core−shell structure (with the exception of the data at concentrations lower than 0.05 wt %: these data were modeled to a semiflexible chain with excluded volume) and are available from the NCNR.[40] The model consists of a polydisperse spherical core and a shell of constant thickness. This function is useful for vesicles and liposomes because the scattering length density of the core and the solvent can be set to the same value, thus calculating the scattering from a spherical shell with constant thickness, but polydisperse inner radius. We refer the interested reader to a paper by Bartlett, which describes the mathematical interpretation of this model.[41]

Results and Discussion

Low Concentrations: c < 0.05 wt %. At concentrations lower than 0.05 wt %, wormlike micelles are observed over a broad temperature range. Figure 1 shows the SANS data for 0.0025% EO_6BO_{11} (by mass fraction) in D_2O at 30 °C, with the corresponding fir to a semiflexible chain with excluded volume. The parameters extracted from this fit are the following: a contour length, $L = 1400 \pm 100$ Å, a Kuhn length, $b = 70 \pm 3$ Å, and a radius, $R = 39.0 \pm 0.5$ Å. However, this article concentrates on vesicle structures and we do not discuss this further. Such effects of temperature on wormlike micelles have been reported for $EO_{18}BO_9$ and the interested reader is referred to this prior publication and references therein.[23]

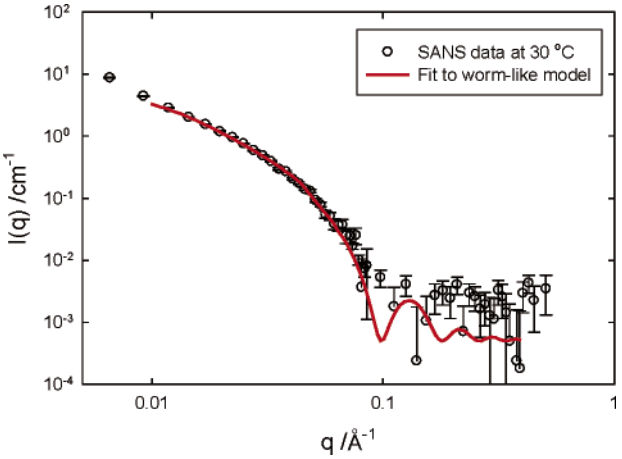

Figure 1. SANS intensity as a function of wave vector, $I(q)$, of 0.0025% (by mass fraction) EO_6BO_{11} at 30 °C. The red solid line represents the fit to a wormlike micelle model. For clarification purposes only every third data point has been plotted.

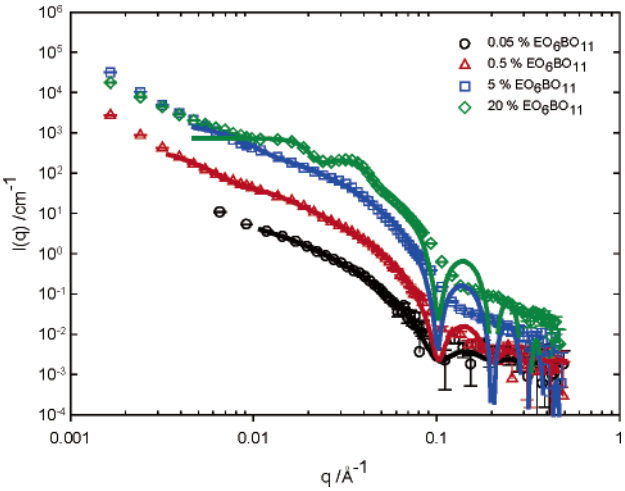

Figure 2. The SANS profiles (open circles) with fits (solid lines) to the polydisperse core−shell model for 0.05%, 0.5%, 5.0%, and 20.0% (by mass fraction) EO_6BO_{11} in D_2O at 30 °C. For clarification purposes only every third data point has been plotted.

Increased Concentrations: 0.05 wt % < c < 20 wt %. *Effect of Concentration.* In this section we show the changes in structure as the concentration of EO_6BO_{11} is changed at constant temperature.

Figure 2 shows the SANS data (with respective fits to eq 5) for a variety of concentrations (0.05% to 20.0%) of EO_6BO_{11} in D_2O at 30 °C. At low q, the scaling of $I(q)$ of q^{-2} is indicative of a vesicle structure.[33] One may expect the SANS profile to have a low q scaling of $I(q)$ scaling as q^0 (describing the Guinier region of the curve) since the shape of the scattering particles is spherical.[44] However, the vesicle shell is thin in comparison to the overall vesicle radius, resulting in the scattering pattern probing flat lamellae on a local scale over the low q range. The fits to the polydisperse core−shell model are shown in Figure 2 as solid lines. The fit to the data at 0.05% EO_6BO_{11} shows good agreement, especially in the low q region of the scattering profile; a slope in $I(q)$ of q^{-2} and smeared out oscillations in the form factor are all consistent with relatively small polydisperse vesicles. At higher q, there is a discrepancy between the data and the model. This is due to polydispersity in vesicle shell thickness, which the model does not account for. We conclude that there is a polydispersity not only in vesicle radii but also in shell thickness. The thickness, t, of the vesicles varies only slightly on increasing concentration as stated in Table 1. As

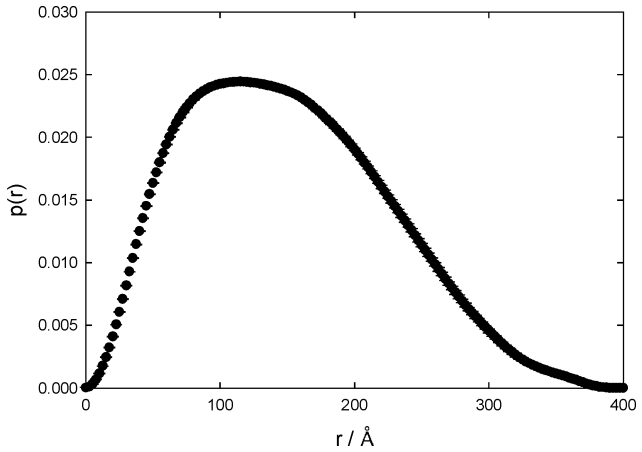

Figure 3. Pair distance distribution function, $p(r)$, for 0.5% (by mass fraction) of EO_6BO_{11} in D_2O at 30 °C. The respective fit to the $I(q)$ data is shown in Figure 2.

TABLE 1: Vesicle Dimensions (Core Radius, R_{core}, and Shell Thickness, t) and Polydispersity As Determined from SANS Modeling for Different Concentrations of EO_6BO_{11} in D_2O at 30 °C

$[EO_6BO_{11}]$ (% mass fraction)	R_{core} (Å)	t (Å)	polydispersity
0.05	155.91 ± 33.1	60.055 ± 1.480	0.51384 ± 0.114
0.5	219.25 ± 3.65	61.349 ± 0.259	0.40623 ± 0.00795
5.0	123.76 ± 2.31	62.368 ± 0.132	0.45103 ± 0.0109
20.0	90.34 ± 0.172	62.015 ± 0.0788	0.23099 ± 0.00682

the concentration is increased 10-fold to 0.5% the overall scattered intensity increases. We explain this increase in intensity by an increased concentration of vesicles. Similarly, the intensity of scattered radiation is increased when the polymer concentration is increased to 5.0%. However, at 20% polymer, this scaling of scattered intensity with concentration is no longer observed in the low q portion of the SANS profile. In the low q region, the structure factor $S(q)$ becomes increasingly dominant at higher concentrations, and at 20% the $S(q)$ brings about a reduction in overall scattered intensity at low q. However, we point out that at high q (where $S(q)$ contributions are significantly reduced), the scaling of scattered intensity with polymer concentration is evident for all concentrations probed.

The indirect Fourier transformation of the observed scattered intensity leads to the pair distance distribution function, $p(r)$. Figure 3 shows this function for 0.5% EO_6BO_{11} at 30 °C. The corresponding data in reciprocal space (i.e. $I(q)$ vs q) are shown in Figure 2. The peak maximum corresponds to the most likely vesicle radius. The point at which the function falls back to zero is the maximum particle dimension, D_{max}. We know that the vesicles formed are of different sizes, so we do not pay strict attention to the dimensions determined from this method of analysis. What we do conclude from the $p(r)$ profile, however, is the shape of the scattering particles. A perfectly spherical particle will have a perfectly symmetric function about a central maximum. The $p(r)$ profile determined from our small angle scattering data shows a function that has a degree of asphericity associated with it. This asymmetry could mean that the vesicles are ellipsoidal, but this is more likely to be due to the polydispersity associated with the vesicle size.

The work of Harris et al. [27] shows that multilamellar vesicles are in existence over the concentration range of our interest: 0.05% to 20% by mass fraction for several EO_nBO_m block copolymers in water, including EO_6BO_{11}. Harris et al. measured the vesicle diameter on the polymer $EO_{11}BO_{11}$. This polymer formed MLVs with diameters ranging from 3 to 30 μm (a mean vesicle diameter of 5.1 μm was determined). Harris noted that on filtering these solutions through either 5 or 0.45 μm Nylon filters, a mean vesicle size of 70 nm was then obtained. It was suggested that this size was the minimum size for a stable vesicle and was possibly the limiting size for ULVs. It should be pointed out that prior to any SANS experiments the EO_6BO_{11} samples we used were filtered. It is therefore not surprising that our SANS data reveal vesicle sizes ranging from 30 to 60 nm (depending on polymer concentration), which we attribute to scattering from ULVs. The vesicle dimensions are smaller than those observed by Harris et al. We attribute this to the reduced ethylene oxide block length. The same polymer (EO_6BO_{11}) has also been used as a system to study in a continuous flow microfluidic small-angle light scattering system.[42] This experiment, performed on unfiltered polymer solutions, has identified MLV structures of sizes between 2 and 20 μm. These dimensions are consistent with measurements performed by Harris on unfiltered polymer vesicles (where the diameter ranges from 3 to 30 μm for $EO_{11}BO_{11}$). The sample system has been studied by simultaneous SAXS/WAXS and a broad peak corresponding to domains of approximately 100−120 Å was identified.[43] This peak has been attributed to correlations between adjacent lamellae: either in the same vesicle (as part of a MLV) or adjacent vesicles whose shells are these distances apart (i.e., a network of closely packed vesicles). From our observations using SANS (and our prior scattering studies[42,43]) and the observations made by Harris using microscopy, we can comfortably conclude that the polymer EO_6BO_{11} readily forms a mixture of ULVs and MLVs over a wide concentration range (0.05% to 20% by mass fraction) in D_2O.

Battaglia and Ryan recently reported that the self-assembly of block copolymers of this type ($EO_{16}BO_{22}$, $EO_{50}BO_{70}$, $EO_{68}BO_{65}$, $EO_{115}BO_{103}$, $BO_{37}EO_{77}BO_{37}$, $BO_{46}EO_{99}BO_{46}$, $EO_{31}BO_{54}EO_{31}$, $EO_{34}BO_{75}EO_{34}$, $EO_{40}BO_{100}EO_{40}$, and $EO_{32}BO_{114}EO_{32}$) can form unilamellar and multilamellar vesicles.[45] The difference in our findings is that EO_6BO_{11} forms a mixture of both ULVs and MLVs at room temperature in water, with no electroagitation or mechanical agitation. Bataglia and Ryan report that the larger micron sized MLVs are produced by the application of an AC field to electrodes that contain a chloroform solution of the block copolymer. The nanoscale vesicles were generated by rehydration of an evaporated chloroform solution of polymer. The resulting solution was then extruded through a polycarbonate membrane. We have shown that the separation of nanoscale ULVs from the solution of coexisting ULVs and MLVs in EO_6BO_{11} may be carried out by such filtration techniques. The advantage of the EO_6BO_{11} system is that these structures are easily formed in water, at room temperature with no need for rehydration from a chloroform solution.

Effect of Temperature. In this section we describe the changes in bilayer structure from spherical vesicles to planar lamellae as the temperature is increased.

The vesicle structure of EO_6BO_{11} is clearly affected by a change in temperature. This is illustrated in Figure 4a−d, which shows the SANS profiles for 0.05%, 0.5%, 0.05%, 5%, and 20% EO_6BO_{11} (by mass fraction) in D_2O, at temperatures of 30 to 90 °C. At 0.05% (Figure 4a), the structure is shown to be relatively stable up to 90 °C, where the vesicle structure collapses. The characteristic q^{-2} scaling of $I(q)$ is no longer evident, and a small broad correlation peak is observed. This effect is more pronounced in Figure 4b−d. Figure 4b shows the SANS profiles for 0.5% EO_6BO_{11} in D_2O. Once again, the vesicle structure is stable under moderate heating, but at 80 °C,

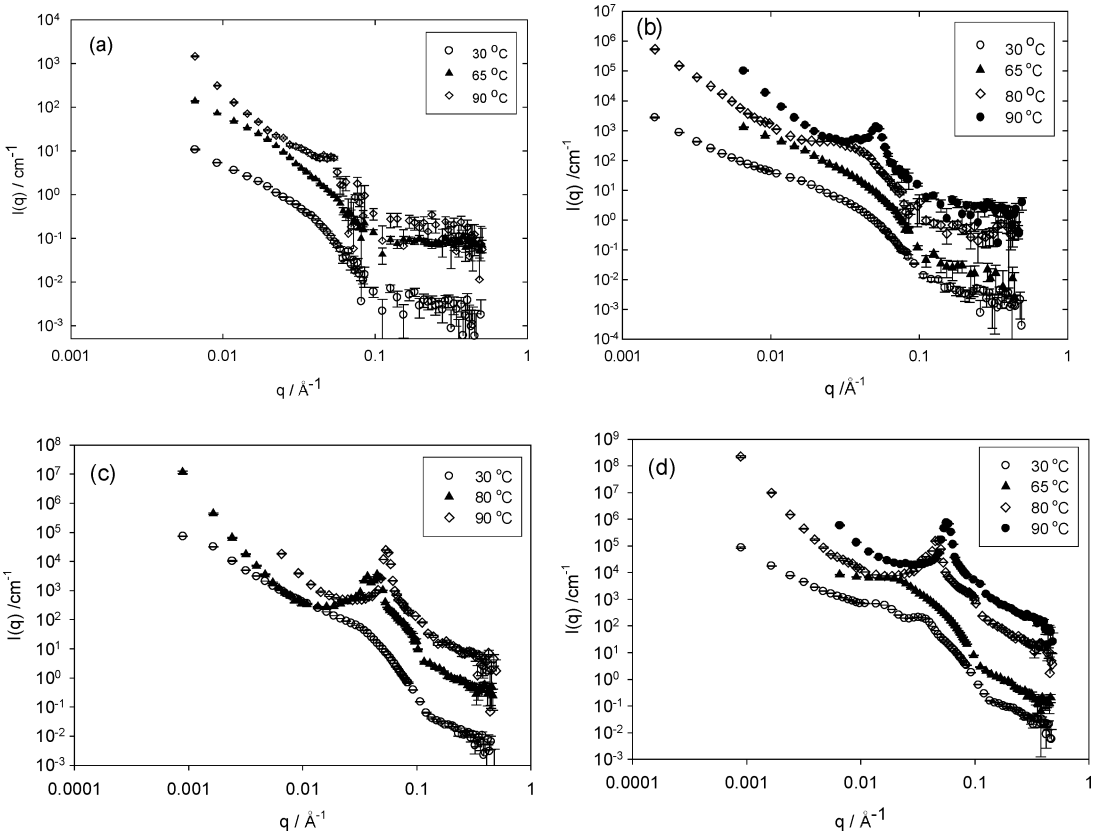

Figure 4. (a) The SANS profiles for 0.05% (by mass fraction) of EO_6BO_{11} in water at 30 (open circles), 65 (solid triangles), and 90 °C (open diamonds). Data have been shifted along the *y*-axis for clarity (shifted by a factor of 10 for the 65 °C data and by a factor of 50 for the 90 °C data). (b) The SANS profiles for 0.5% (by mass fraction) of EO_6BO_{11} in water at 30 (open circles), 65 (solid triangles), 80 (open diamonds), and 90 °C (solid circles). Data are shifted by factors of 1, 10, 100, and 1000, respectively. (c) The SANS profiles for 5% (by mass fraction) of EO_6BO_{11} in water at 30 (open circles), 80 (solid triangles), and 90 °C (open diamonds). Data are shifted by factors of 1, 100, and 1000, respectively. (d) The SANS profiles for 20% (by mass fraction) of EO_6BO_{11} in water at 30 (open circles), 65 (solid triangles), 80 (open diamonds), and 90 °C (solid circles). Data are shifted by factors of 1, 100, 1000, and 10000, respectively. For clarification purposes, only every third data point was plotted.

a peak at ~0.03 $Å^{-1}$ is observed, corresponding to an increase in concentration of vesicles and therefore increased resolution. As the temperature is increased to 90 °C, this peak shifts to a larger *q* value (~0.05 $Å^{-1}$), corresponding to a domain spacing of ~125 Å. We believe this is due to the curvature of the lamellae becoming reduced at elevated temperatures, providing a stronger correlation between adjacent lamellae. We postulate that on increasing the temperature, the vesicles fuse to form a planar lamellar structure with reduced domain spacing.

Figure 4c shows the formation of a lyotropic liquid crystalline phase for a concentration of 5% at elevated temperatures. At 80 °C there are substantial differences in the SANS profile when compared with data recorded at lower temperatures. At 80 °C several peaks are observed. We attribute the "peak-splitting" shown at 80 °C to a biphasic region, of different length scales: 134.5 ± 0.2 and 166.0 ± 0.2 Å. There are higher order peaks present, but the limited resolution renders phase identification very difficult. A technique such as SAXS may be able to decipher the structure in this case. On heating further to 90 °C the domain spacing is reduced to 115.0 ± 0.2 Å. A second peak is observed. The peaks are in the positional ratio q^*:$2q^*$, indicative of planar lamellae.

On increasing the concentration to 20% planar lamellar structures are also formed at higher temperatures. The domain spacing observed is 135.0 ± 0.2 Å at 80 °C and 110.0 ± 0.2 Å at 90 °C. This is comparable to those dimensions determined for 5% polymer. Our data at 65 °C show the disappearance of the two peaks that are initially observed at 30 °C. As mentioned previously, these two peaks are due to the form factor (arising from the shape of the vesicles). Our data suggest that at 65 °C the concentration of these vesicles decreases. However, on heating to 80 °C and higher, the block copolymer that appears forms a planar lamellar structure, characterized by peaks observed in the positional ratio of q^*:$2q^*$.

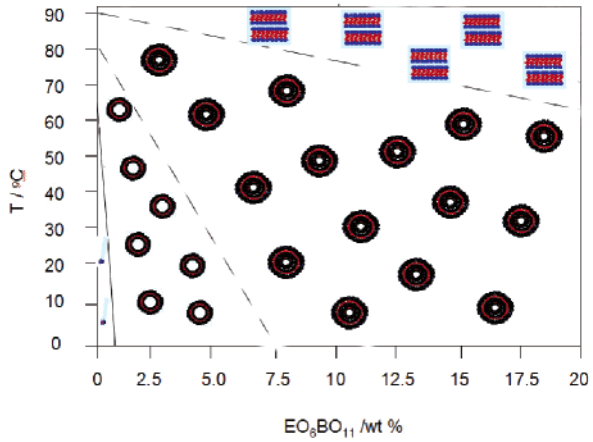

Figure 5. Morphologies observed by EO_6BO_{11} in D_2O as a function of concentration and temperature. The dotted lines represent estimated boundaries between the different bilayer structures. The solid line represents the phase transition between worm-like micelles and vesicles.

Figure 5 illustrates the morphologies adopted for the block copolymer EO_6BO_{11} in D_2O over the concentration range 0−20 wt % at temperatures of 10−90 °C. This phase diagram is partially constructed not only from this study, but from previous

studies on the MLV formation of EO_6BO_{11} in H_2O.[42,43] We show that at very low concentration and temperature, wormlike micelles are in existence. As the concentration is increased to 0.05%, vesicles form. These vesicles are stable up to 20% polymer and high temperatures. The present SANS study, combined with our previous studies[42,43] and the study by Harris,[27] provides strong evidence to suggest a coexisting population of ULVs and MLVs. It is likely that in the higher concentrations of this range, MLV structures are favored, whereas ULV structures are favored in the lower concentration regime. The dotted lines in Figure 5 are for visual aid only and are estimates that should not be taken literally.

Conclusions

We show that vesicles from the diblock copolyether, EO_6BO_{11}, are spontaneously formed under favorable conditions, i.e., at room temperature, at atmospheric pressure, and under zero shear in water. The vesicles formed are likely to be a coexistence of both small nanoscale ULVs and large micron-sized MLVs. At a polymer concentration of 0.05%, the solution is close to the critical vesicle concentration and the SANS data fit reasonably well to a ULV model. An indirect Fourier transformation of the SANS data gives the $p(r)$ function which, as expected, shows the vesicles to be spherical. The vesicles are most likely unilamellar of diameter 300−600 Å with a shell thickness of approximately 60 Å, depending on temperature and concentration. Such observations are consistent with those determined by Harris for a similar block copolymer, $EO_{11}BO_{11}$. We confirm that filtering the polymer solutions separates the MLV and ULV structures. It is possible that some MLVs exist in this sample because there sizes are so big that they fall out of the range of detection by conventional SANS measurements. However, if MLV structures were to exist, a correlation between adjacent lamellae would be shown and this is not observed in our data. Our data fit well to a ULV model.

At higher concentrations and temperatures the vesicle concentration increases. A thermally induced vesicle to lyotropic liquid crystal phase is observed at 80 °C for 5% and 20% EO_6BO_{11}. We anticipate that the increase in temperature causes the solvent (D_2O) to become a poorer solvent for the hydrophilic EO blocks, increasing the overall hydrophobic character of the polymer network and leading to the formation of planar lamellae.

We have successfully identified the unilamellar vesicle phases present for EO_6BO_{11} in D_2O by SANS. This work complements studies on the multilamellar structures of EO_6BO_{11} that were identified by microscopy techniques and small-angle light scattering.[27,43] To the authors knowledge this is the first reported polymer that spontaneously forms both ULVs and MLVs under such conditions.

Acknowledgment. The authors wish to acknowledge Dr. S. Lin-Gibson for her kind assistance during the SANS experiments, and the Center for Neutron Research (NCNR) at the National Institute of Standards and Technology (U.S Department of Commerce) for the allocation of the SANS beamtime. The authors also wish to thank Dr. Keith Harris at Dow Chemicals for providing the polymer samples and Dr. Srinivasa Raghavan at UMD for his useful comments.

References and Notes

(1) Lasic, D. D. In *Vesicles*; Rossoff, M., Ed.; Marcel Dekker: New York, 1996; p 448.

(2) Allen, C.; Maysinger, D.; Eisenberg, A. *Colloids Surf. B* **1999**, *16*, 3.

(3) Ding, J.; Liu, G. *J. Phys. Chem. B* **1998**, *102*, 6107.

(4) Derici, L.; Ledger, S.; Mai, S.; Booth, C.; Hamley, I. W.; Pedersen, J. S. *Phys. Chem. Chem. Phys.* **1999**, *1*, 2773.

(5) Li, H.; Yu, G.-E.; Price, C.; Booth, C.; Fairclough, J. P. A.; Ryan, A. J.; Mortensen, K. *Langmuir* **2003**, *19*, 1075.

(6) Hamley, I. W.; Mai, S.; Ryan, A. J.; Fairclough, J. P. A.; Booth, C. *Phys. Chem. Chem. Phys.* **2001**, *3*, 2972.

(7) Pople, J. A.; Hamley, I. W.; Fairclough, J. P. A.; Ryan, A. J.; Komanscheck, B. U.; Gleeson, A. J.; Yu, G.-E.; Booth, C. *Macromolecules* **1997**, *30*, 5721.

(8) Yu, G.-E.; Li, H.; Fairclough, J. P. A.; Ryan, A. J.; McKeown, N.; Ali-Adib, Z.; Price, C.; Booth, C. *Langmuir* **1998**, *14*, 5782.

(9) Kelarakis, A.; Havredaki, V.; Yu, G.-E.; Derici, L.; Booth, C. *Macromolecules* **1998**, *102*, 1149.

(10) Zipfel, J.; Berghausen, J.; Schmidt, G.; Lindner, P.; Alexandridis, P.; Tsianou, M.; Richtering, W. *Phys. Chem. Chem. Phys.* **1999**, *1*, 3905.

(11) Diat, O.; Nallet, F.; Roux, D. *J. Phys. II* **1993**, *3*, 1427.

(12) Bergenholtz, J.; Wagner, N. *Langmuir* **1996**, *12*, 3122.

(13) Zipfel, J.; Lindner, P.; Tsianou, M.; Alexandridis, P.; Richtering, W. *Langmuir* **1999**, *15*, 2599.

(14) Gerasimov, O. V.; Rui, Y.; Thompson, D. H. In *Vesicles*; Rosoff, M., Ed.; Marcel Dekker: New York, 1996; p 682.

(15) Discher, B. M.; Won, Y. Y.; Ege, D. S.; Lee, J. C.-M.; Bates, F. S.; Discher, D. E.; Hammer, D. A. *Science* **1999**, *284*, 1143.

(16) Yu, K.; Eisenberg, A. *Macromolecules* **1996**, *29*, 6359.

(17) Luo, L.; Eisenberg, A. *Langmuir* **2001**, *17*, 6804.

(18) Zhang, L.; Eisenberg, A. *Polym. Adv. Technol.* **1998**, *9*, 677.

(19) Zhang, L.; Eisenberg, A. *Macromolecules* **1999**, *32*, 2239.

(20) Gomati, R.; Appell, J.; Bassereau, P.; Marigan, J.; Porte, G. *J. Phys. Chem.* **1987**, *91*, 6203.

(21) Platz, G.; Thunig, C.; Pölike, J.; Kirchhoff, W.; Nickel, D. *Colloids Surf. A* **1994**, *88*, 113.

(22) Israelachvili, J. N. *Intermolecular and Surface Forces*; Academic: New York, 1992; pp 380−384.

(23) Norman, A. I.; Ho, D. L.; Karim, A.; Amis, E. J. *J. Coll. Interface Sci.* **2005**, *288*, 155.

(24) Yu, G.-E.; Yang, Y.-W.; Yang, Z.; Attwood, D.; Booth, C. *Langmuir* **1996**, *14*, 3404.

(25) Gradzielski, M. *J. Phys.*: *Condens. Matter* **2003**, *15*, R655.

(26) Regev, O.; Guillemet, F. *Langmuir* **1999**, *15*, 4357.

(27) Harris, J. K.; Rose, G. D.; Bruening, M. L. *Langmuir* **2002**, *18*, 5337.

(28) Rayleigh, J. W. S. *Proc. R. Soc. London, Ser. A* **1911**, *84*, 25.

(29) Pedersen, J. S. *Analysis of small angle scattering data*: *Modeling and least squares fitting*, European Summer School on Small Angle Scattering, Lecture Notes, Bombannes, France, 1996.

(30) Fournet, G. *Bull. Soc. Fr. Mineral. Cristallogr.* **1951**, *74*, 39.

(31) Richards, R. W. *Adv. Polym. Sci.* **1985**, *71*, 1.

(32) Mittelbach, P.; Porod, G. *Acta Phys. Aust.* **1961**, *14*, 185.

(33) Kratky, O.; Porod, G. *Recl. Trav. Chim. Pays-Bas* **1949**, *68*, 1106.

(34) Glatter, O. The Inverse Scattering Problem in Small-Angle Scattering. In Neutrons, X-rays, and Light: Scattering methods applied to soft condensed matter; Lindner, P., Zemb, T., Eds.; Elsevier: Amsterdam, The Netherlands, 2000.

(35) Sadler, D. M.; Worcester, D. L. *J. Mol. Biol.* **1982**, *159*, 485.

(36) Riberio, A. A.; Dennis, E. A. In *Non-ionic surfactants*: *Physical Chemistry*; Shick, M. J., Ed.; Marcel Dekker: New York, 1987; pp 975−979.

(37) Glinka, C. J.; Barker, J. G.; Hammouda, B.; Krueger, S.; Moyer, J. J.; Orts, W. J. *J. Appl. Crystallogr.* **1998**, *31*, 430.

(38) *NG3 and NG7 30 m SANS Instrument Data Acquisition Manual*; Cold Neutron Research Facility at the National Institute of Standards and Technology, 1999.

(39) Porod, G. *Kolloid-Z* **1951**, *124*, 83.

(40) http://www.ncnr.nist.gov/resources/index.html

(41) Bartlett, P.; Ottewill, R. H. *J. Chem. Phys.* **1992**, *96*, 3306.

(42) Norman, A. I.; Zhang, W.; Beers, K. L.; Amis, E. J. *J. Colloid Interface Sci.* Submitted for publication.

(43) Norman, A. I.; Cabral, J. T.; Karim, A.; Amis, E. J. *Macromol. Rapid Commun.* **2004**, *25*, 307.

(44) Grazielski, M.; Muller, M.; Bergmeier, M.; Hoffmann, H.; Hoinkis, E. *J. Phys. Chem. B* **1999**, *103*, 1416.

(45) Battaglia, G.; Ryan, A. J. *J. Am. Chem. Soc.* **2005**, *127*, 8757.